PNAS

Supporting Information for

A nemaline myopathy-linked mutation inhibits the actin-regulatory functions of tropomodulin and leiomodin

Lauren E. Schultz, Mert Colpan, Garry E. Smith Jr., Rachel M. Mayfield, Tania M. Larrinaga, Alla S. Kostyukova, Carol C. Gregorio

Carol C. Gregorio

Email: gregorio@email.arizona.edu

This PDF file includes:

SI MATERIALS AND METHODS

Plasmid construction and site-directed mutagenesis.

cDNA from mouse hearts was used to clone full-length mTmod1, mLmod2, and mLmod3 (NCBI Reference Sequences: NP_068683.1, NP_444328.1, and NP_001074626.1, respectively). The coding sequences from mTmod1 was subcloned into pEGFP-C1 (Clontech, Mountain View, CA) (1), and mLmod2 or mLmod3 was subcloned into pEGFP-C2 using *Xho*I and *Hin*dIII restriction sites. The G-to-R mutation was introduced into mTmod1, mLmod2, and mLmod3 by amplifying respective WT Tmod1/Lmod2/Lmod3 plasmids via PCR following the QuikChange™ site-directed mutagenesis protocol (2) in the presence of following primer sequences:

Tmod1 [G268R] Forward primer: 5'-TCTCTGGAGCTCGGATCCTGCGCCTGGTGGAAG-3'
Tmod1 [G268R] Reverse primer: 5'-GCGCAGGATCCGAGCTCCAGAGATGAAGTTGGACTC-3'
Lmod2 [G291R] Forward primer: 5'-TGGCAAGCGGATCCTGGCCATCATGAGAGCCCTGC-3'
Lmod2 [G291R] Reverse primer: 5'-CAGGATCCGCTTGCCAGTGATGAAGTTGGACTCCACGT-3'
Lmod3 [G337R] Forward primer: 5'-ACTGGGAACGGCATCGTGGCCATCATGAGGTGCCTC-3'
Lmod3 [G337R] Reverse primer:
5'-GCCACGATGCCGTTCCCAGTGATGAAGTTGGACTCAATATTGAGGGTGG-3'

Underlined are the substituted nucleotides. After generating the PCR product with the mutation, the remaining WT template was digested with *DpnI* (New England Biolabs) and the mixture was used to transform DH5α *E. coli* cells (Life Technologies, Carlsbad, CA). Clones resistant to kanamycin were examined for the mutation and plasmid DNA was purified using ZR Plasmid Miniprep Classic kit (Zymo Research, Irvine, CA). DNA Sanger sequencing performed by Eton Bioscience, Inc. (San Diego, CA).

GSN-bio-His plasmid encoding human plasma gelsolin (hGSN) was a gift from Gavin Wright (Addgene plasmid #52067; http://n2t.net/addgene:52067; RRID:Addgene_52067) (3) hGSN with a C-terminal 6xHistidine-tag and full-length or LRR domains of mTmod1, mLmod2 and the LRR domain of mLmod3 with an N-terminal 6xHistidine-tag were cloned into pReceiver-B01 plasmid (GeneCopoeia, Rockville, MD), whereas full-length mLmod3 with an N-terminal 6xHistidine-tag was cloned into pTYB3 (New England Biolabs) for recombinant protein expression. Recombinant rat striated muscle α-Tpm (rTpm1.1) with an N-terminal Ala-Ser extension in pET11d expression plasmid was a generous gift from Dr. Sarah Hitchcock-DeGregori (Rutgers University, Piscataway, NJ).

Protein expression and purification

Globular actin (G-actin) was purified from actin acetone powder (4) obtained from rabbit skeletal muscle as described elsewhere (5). Recombinant Tpm1.1 with Ala-Ser extension on its N-terminus to mimic acetylation of Tpm was purified as described previously (6). hGSN was purified as described previously (7) and dialyzed into 10 mM Tris-HCl, pH 7.5, 150 mM NaCl, 0.1 mM $MgCl_2$.

WT and mutant mLmod3 were purified as described previously (8). Full-length mTmod1 or mLmod2 and LRR fragments of mTmod1, mLmod2 or mLmod3 were expressed and purified as previously described in (6) with modifications. Briefly, BL21 Rosetta™ 2 (DE3) pLysS cells (Novagen) transformed with mTmod1, mLmod2, mLmod3 constructs were grown at 37°C in LB media with 0.1 mg/mL ampicillin and 0.05 mg/mL chloramphenicol that was supplemented with 0.4 mM IPTG for induction at OD_{600} = 0.6. The cells were grown for 4-5 hr at 37°C after induction and pelleted at 5,000xg, 4°C, 15 min. The pellets were flash frozen with liquid nitrogen and stored at -80°C until processing. Pellets were then resuspended according to manufacturer's recommendations for using the B-PER® Bacterial Protein Extraction Reagent (Thermo Fisher) in the presence of 0.1 mg/mL lysozyme (Sigma) and 1x Halt™ protease inhibitor cocktail, sonicated, and spun down at 16,000 RPM (Beckman-Coulter JA-17 Rotor), 4°C, 30 min. mTmod1, mLmod2 or mLmod3 in inclusion bodies in the pellets were solubilized by resuspending pellets in 100 mM sodium phosphate pH 8.0 (pH 7.0 for mTmod1 LRR), 300 mM NaCl and 10 mM Imidazole with 8 M Urea (column buffer) overnight at 4°C on ice. The resuspension was centrifuged at 16,000 RPM (Beckman-Coulter JA-17 Rotor), 4°C, 30 min and the supernatant was loaded onto Ni-NTA agarose Superflow resin (Qiagen). Proteins were eluted

with column buffer including 250 mM imidazole and dialyzed stepwise against Urea (8 M to 0 M Urea in 2 M steps) overnight at 4°C in 20 mM Tris-HCl, 150 mM NaCl 1 mM EDTA for mTmod1 (pH 7.0) and mLmod2 (pH 8.0), or 100 mM sodium phosphate pH 8.0, 10 mM Tris-HCl, 300 mM NaCl for mLmod3 LRR. Purified proteins were concentrated using Vivaspin® 15R centrifugal concentrators (Fisher Scientific) and protein concentration was determined by Pierce™ BCA protein assay kit according to manufacturer's recommendations. Proteins were flash frozen in liquid nitrogen and stored at -80°C until experiments.

Molecular dynamics simulations

Molecular visualization and structure editing was performed using UCSF Chimera (27), and LEaP. Complexes were neutralized with Na^+ ions and solvated in a cuboid box of TIP3P water, with at least 10 Å between any atom in the molecule and the edge of the box and with 0.75 Å between any water atom and any other atom. Histidine protonation states were set to neutral. The MDS were performed in Amber18 (28) with the ff14SB forcefield (29) and constant pressure periodic boundary conditions. Energy minimization was performed by 2500 cycles of the steepest descent method followed by 2500 cycles of the conjugate gradient method. Temperature was controlled at 310K with the Berendsen thermostat with a time constant of 1.0 ps. Pressure was controlled by the Berendsen barostat with isotropic scaling and a 1.0 ps relaxation time. The cutoff value for non-bonded interactions was set to 8 Å. Covalent bonds involving hydrogens were constrained by SHAKE and omitted from calculation. The time step was 1 fs and the total simulation time was 400 ns. Root mean squared deviations and distance time-courses were calculated in cpptraj (43). Crystal structures of Tmod1 and Lmod2 in complex with actin were taken from the Protein Data Bank (PDB) https://www.rcsb.org/. WT LRR domains were obtained by deleting gelsolin, actin, ATP, and ions from PDB ID codes: 4PKI and 5WFN. Resultant structures of the mutated Tmod1 and Lmod2 LRRs were aligned with the WT LRRs of the crystal structures (PDB ID codes: 4PKI and 5WFN respectively), after which WT LRRs were deleted. Distances between select atoms in the new mutated LRR/actin complexes were calculated. Distances between atoms participating in hydrogen bonding within the asparagine ladders of the LRR domains were calculated at 50 ps intervals over the entire 400 ns trajectory, and the 2.5 ns moving average plotted An upper cutoff of 2.5 Å (43) was used to judge whether the atoms remained in the hydrogen bond. The bonds are numbered according to their appearance in the sequence from the N-terminus.

Limited proteolysis

Limited proteolysis was performed by mixing 20 µg Tmod1, Lmod2, and Lmod3 WT or G-to-R mutant LRR domains with 0.4 µg *Staphylococcus aureus* V8 protease (Worthington Biochemical, Lakewood, NJ) in 100 mM sodium-phosphate pH 7.8 at 20°C. Samples for SDS-PAGE were prepared before mixing (time 0) and after incubation with V8 protease for 1, 5, 20, 60 and 120 minutes (min.), as well as after overnight incubation (~16 hrs). V8 protease was inactivated after adding 1x Laemmli sample buffer and boiling samples at 100°C for 10 min. Samples were then flash frozen in liquid nitrogen and stored at -80°C. Samples were loaded on to 15% SDS-acrylamide gels and Coomassie Blue-stained gels were imaged after destaining with LI-COR Odyssey CLx imaging system and analyzed using LI-COR Image Studio Lite™ (LI-COR Biosciences, Lincoln, NE).

Adeno-associated virus generation

Adeno-associated virus (AAV) was generated by the insertion of GFP, GFP-Lmod3 WT, or GFP-Lmod3 [G337R] into pAAV-MCS with a muscle creatine kinase-specific (CK8e) promoter (9) that was developed by Dr. Steve Hauschka and provided by Dr. Jeffrey Chamberlain (University of Washington). Virus was generated onsite following the protocol described in (10). Vector genomes (1.25×10^{12}) were injected into the pericardial cavity of postnatal day 4 (PD4) *Lmod3*-knockout mice (11). Prior to collection at PD20-22, body weight of the mice was recorded and grip strength and rotarod test measurements were performed. Muscle weights were also taken at the time of collection. Note, the

EDL muscle contains higher mRNA transcript levels for muscle creatine kinase (MCK) than the SOL muscle (12), which potentially leads to differential expression levels of GFP-tagged proteins in these muscle types.

Isolation and transfection of neonatal cardiomyocytes and mouse skeletal muscle tissue.
Rat neonatal cardiomyocytes were cultured on 35-mm tissue-culture dishes containing 12-mm round glass coverslips as described in (10). Cells were transfected within 12 hours (hr) of plating with 1 µg of either GFP, GFP-Tmod1, GFP-Tmod1 [G268R], GFP-Lmod2 WT, or GFP-Lmod2 [G291R], GFP-Lmod3 WT, or GFP-Lmod3 [G337R] DNA using Lipofectamine™ 3000 reagent (Thermo Fisher Scientific, Waltham, MA). 48 hr after transfection, cells were washed with 1X PBS and incubated in relaxing buffer (10 mM 3-(*N*-morpholino) propane sulfonic acid, pH 7.4, 150 mM KCl, 5 mM $MgCl_2$, 1 mM EGTA, and 4 mM ATP) for 15 min and fixed with 2% paraformaldehyde in relaxing buffer for 15 min. Fixed cells were stained for immunofluorescence microscopy as previously described (13). Additionally, extensor digitorum longus (EDL) and soleus (SOL) muscles of mice postnatal day (PD) 20-22 were dissected then stretched and fixed in 4% paraformaldehyde/PBS at 4°C overnight, washed several times with 1X PBS, embedded in Tissue-TEK O.C.T. compound (Fisher Healthcare), and frozen in 2-methlybutane cooled in liquid N_2. 5-µm cryosections were then cut and mounted onto number 1.5 coverslips.

Immunoblotting
EDL and SOL muscles were processed and protein lysate was used for Western blotting following the protocol listed in (10). To control for loading/transfer differences, total lane density of transferred proteins stained with Ponceau S was used. The nitrocellulose membranes were blocked in 5% (wt/vol) nonfat dried milk in 1×TBS for 1 hr at room temperature and incubated with primary antibodies diluted in 2% BSA in 1×TBST overnight at 4 °C. The primary antibodies included rabbit polyclonal anti-LMOD2 (1:1000) (E13; Santa Cruz Biotechnology), rabbit polyclonal anti-LMOD3 (1:1000) (14948-1-AP; Proteintech), and mouse monoclonal anti-GFP (1:5,000) (B-2, Santa Cruz Biotechnology) antibodies. Following 5×10 min 1×TBST washes, the membranes were incubated with fluorescently-labeled secondary antibodies including Alexa Fluor® 690 or Alexa Fluor® 790 AffiniPure anti-rabbit or anti-mouse (1:40,000; Jackson ImmunoResearch) antibodies diluted in 5% (wt/vol) nonfat dried milk in 1×TBST at room temperature for 1.5 hr. Membranes were washed for 5X10 min 1×TBST washes and 1×10 min 1×TBS wash, and then imaged and analyzed using a LI-COR Odyssey CLx imaging system and LI-COR Image Studio Lite™ (LI-COR Biosciences, Lincoln, NE).

Electron microscopy
Intact EDL or SOL muscles were stretched and fixed in a Sylgard (Ellsworth Adhesives, Germantown, WI) dish with a solution containing EM-grade 3.7% paraformaldehyde, 3% glutaraldehyde (Electron Microscopy Sciences) and 0.2% tannic acid in 0.1 M PBS, pH 7.2 for 2 hr at 4 °C. The muscles were then transferred to PBS buffer, dehydrated, and embedded in Araldite/Embed 812 (Electron Microscopy Sciences). 60 nm sections were cut and stained with potassium permanganate and lead citrate followed by observation via transmission electron microscopy (FEI Tecnai Spirit Transmission Electron Microscope).

MHC gels
Myosin heavy chain (MHC) isoforms were separated on 8% acrylamide SDS-gels, run at 275 V, 15 °C for 24 h, followed by staining with Coomassie-Brilliant Blue R-250 (Bio-Rad). After destaining, gel images were captured with an Epson Perfection 2450 Scanner and analyzed with ImageJ (v1.52, NIH). MHC isoform types I and IIB are separated well on gels, but types IIA and IIX overlap, therefore the band(s) corresponding to them is referred to as IIA/IIX. The band for each isotype was determined by running a standard in parallel that consists of a mixture of lysates from WT tibialis cranialis and soleus

muscles, which contains all myosin isoforms in a well-established order (top: IIA/IIX; middle: type IIB; and bottom: type I).

Animal Work

Work with animals was performed under the approval by The Institutional Animal Care and Use Committee at the University of Arizona; Protocol number 08-017, which conformed to all applicable federal and institutional policies, procedures, and regulations, including the PHS Policy on Humane Care and Use of Laboratory Animals, USDA regulations (9 CFR Parts 1, 2, 3), the Federal Animal Welfare Act (7 USC 2131 et. Seq.), the Guide for the Care and Use of Laboratory Animals, and all relevant institutional regulations and policies regarding animal care and use at the University of Arizona.

Statistical Analysis

Prism 9.1.2 (GraphPad Software, Inc., San Diego, CA) was used for compiling the data, generating the figures, and statistical analyses. Two groups were compared using Student's t-test and multiple groups were compared using one-way or two-way ANOVA; differences with $p<0.05$ were considered statistically significant.

Table S1. The G-to-R mutation weakens the actin filament capping and nucleation functions of Tmod and Lmod, respectively. Binding affinities (K_d) and minimal or maximal relative actin polymerization rates were determined from pyrene-actin polymerization experiments in the presence of Tmod or Lmod. Each value is reported as mean ± SD (n=3). Asterisks indicate statistically significant differences from WT Tmod1, Lmod2 or Lmod3 using Student's t-test (*p<0.05, **p<0.01 and ***p<0.001).

	K_d (μM)	Minimal relative polymerization rate
Tmod1	0.33 ± 0.11	0.27 ± 0.04
Tmod1 [G268R]	1.68 ± 0.83*	0.41 ± 0.02**
	K_d (μM)	Maximal relative polymerization rate
Lmod2	0.07 ± 0.02	5.7 ± 0.3
Lmod2 [G291R]	4.34 ± 0.84***	3.4 ± 0.6**
Lmod3	0.04 ± 0.02	3.3 ± 0.04
Lmod3 [G337R]	2.43 ± 1.18*	1.9 ± 0.1**

Table S2. The G-to-R mutation results in loss of contacts formed between LRR domains and actin. Contacts include both hydrogen bonds and salt bridges. Hydrogen bond pairs were considered to be making contact if the distance between them was less than 2.5 angstroms (Å). Salt bridge pairs were considered to be making contact if the distance between them was less than 4 Å.

	Total in WT	Lost	Kept	Added	Total in GR
Tmod1-LRR	16	9			12
			7		
				5	
	Total in WT	Lost	Kept	Added	Total in GR
Lmod2-LRR	15	12			10
			3		
				7	

Table S3. List of residues that lose contact between the LRR domains of Tmod1 or Lmod2 and actin in the presence of the G-to-R mutation.

Location in the LRR	Tmod1	Actin	Location in the LRR	Lmod2	Actin
N-terminal part	Glu-7	Gly-48	Loop 1	Asn-25	Gly-49
	Glu-7	Tyr-55		Asn-25	Lys-51
	Asn-10	Gln-51	Loop 4	Arg-107	Asp-81
				Asn-110	Pro-39
Loop 1	Asn-34	Gln-51	Between Loop 4 and C-terminal helix	Arg-135	Glu-84
	Asn-35	Gly-50		Arg-135	Thr-127
	Asn-35	Lys-52			
Loop 4	Asn-120	Pro-40	C-terminal helix	Thr-150	Lys-119
Between Loop 4 and C-terminal helix	Gly-147	Asn-82		Thr-154	Gln-122
C-terminal Helix	Arg-171	Asp-359		Arg-164	Glu-126
	Arg-174	Glu-127			
	Arg-174	Asp-359		Arg-164	Asp-364

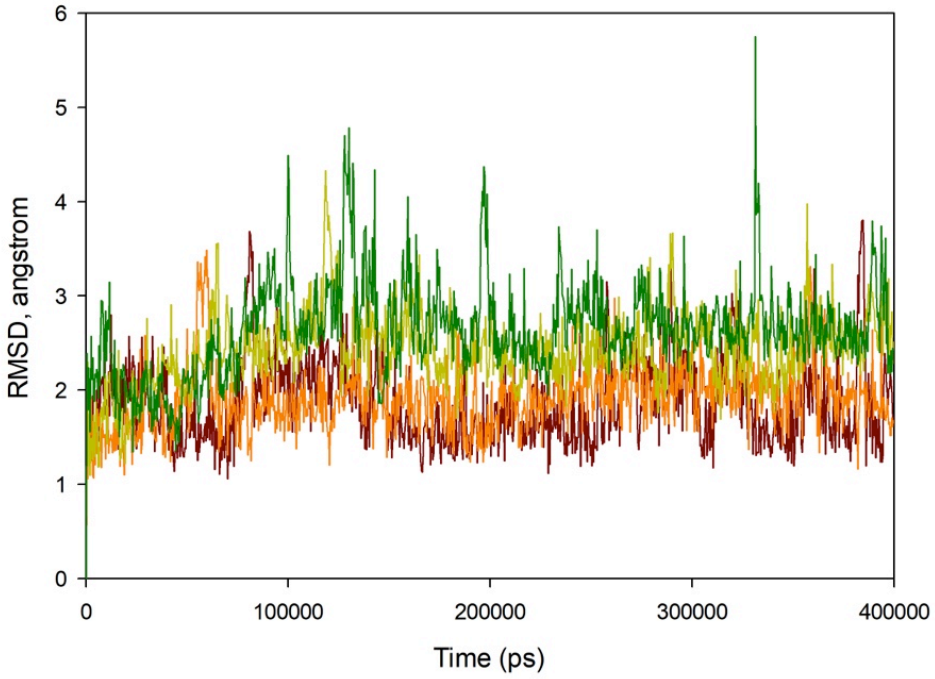

Figure S1: LRR domain of Lmod2 is more flexible than that of Tmod1. Root-mean squared deviation (RMSD) of simulated LRR domains from corresponding crystal structures. Tmod1-LRR is in orange, and the Tmod1-LRR [G268R] is in crimson. Lmod2-LRR is in olive, and Lmod2-LRR [G291R] is in green.

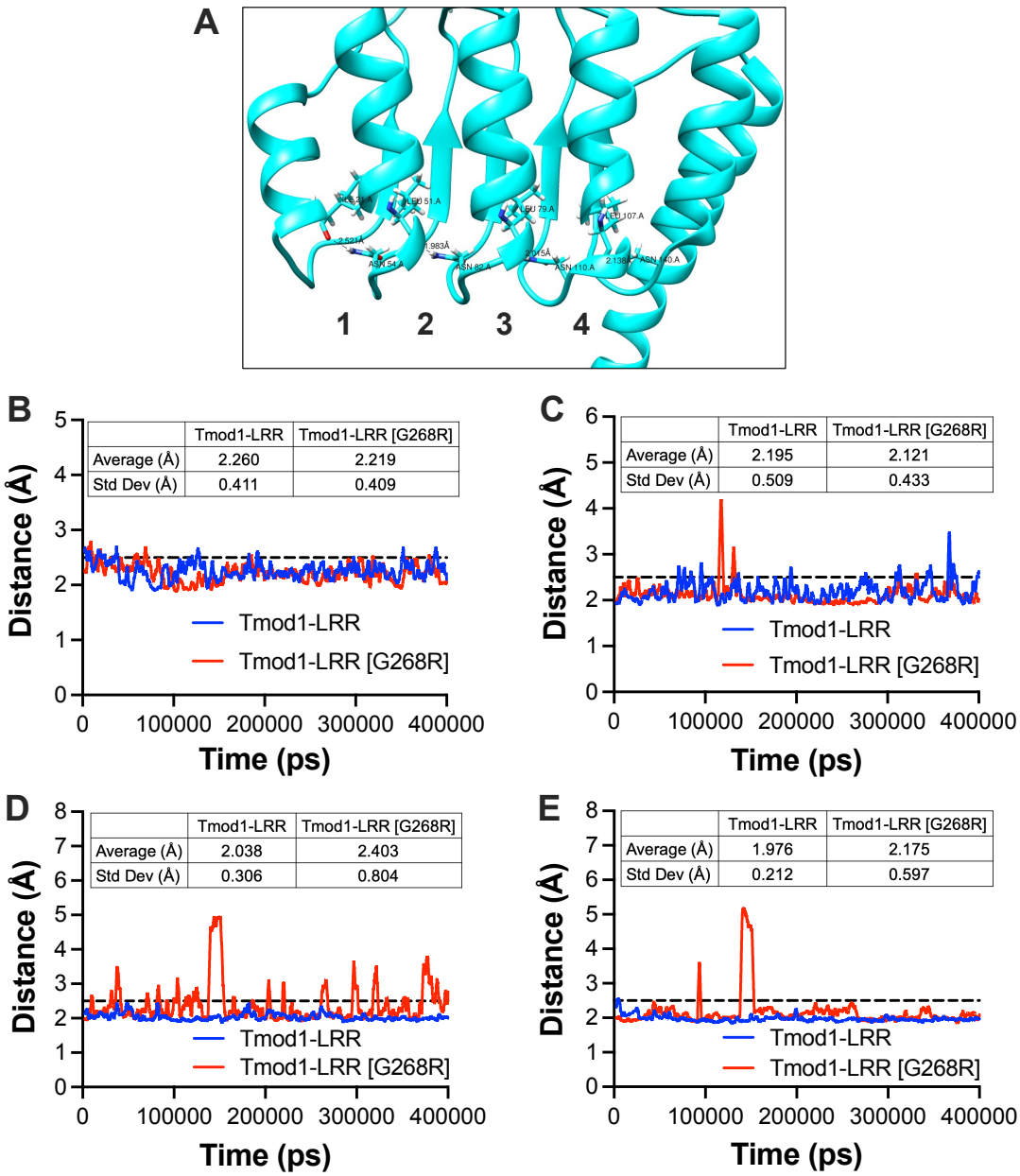

Figure S2: The G-to-R mutation destabilizes certain asparagine ladder hydrogen bonds within the Tmod1 LRR domain. (A) Tmod1-LRR asparagine ladder hydrogen bonds in their crystal structures (PDB ID code: 4PKI). The amino acid residues contributing hydrogen bond donors/acceptors and the distances between these atoms are labeled. Hydrogen bonds (1-4) are numbered based on their appearance in the sequence from the N-terminus. (B-E) Tmod1-LRR and Tmod1-LRR [G268R] asparagine ladder hydrogen bonding atom 2.5 nanoseconds moving average distance. (B) Hydrogen bond 1, (C) Hydrogen bond 2, (D) Hydrogen bond 3, (E) Hydrogen bond 4. Å: angstroms, Std Dev: standard deviation, ps: picoseconds, **- - - -** 2.5 Å H bond cutoff.

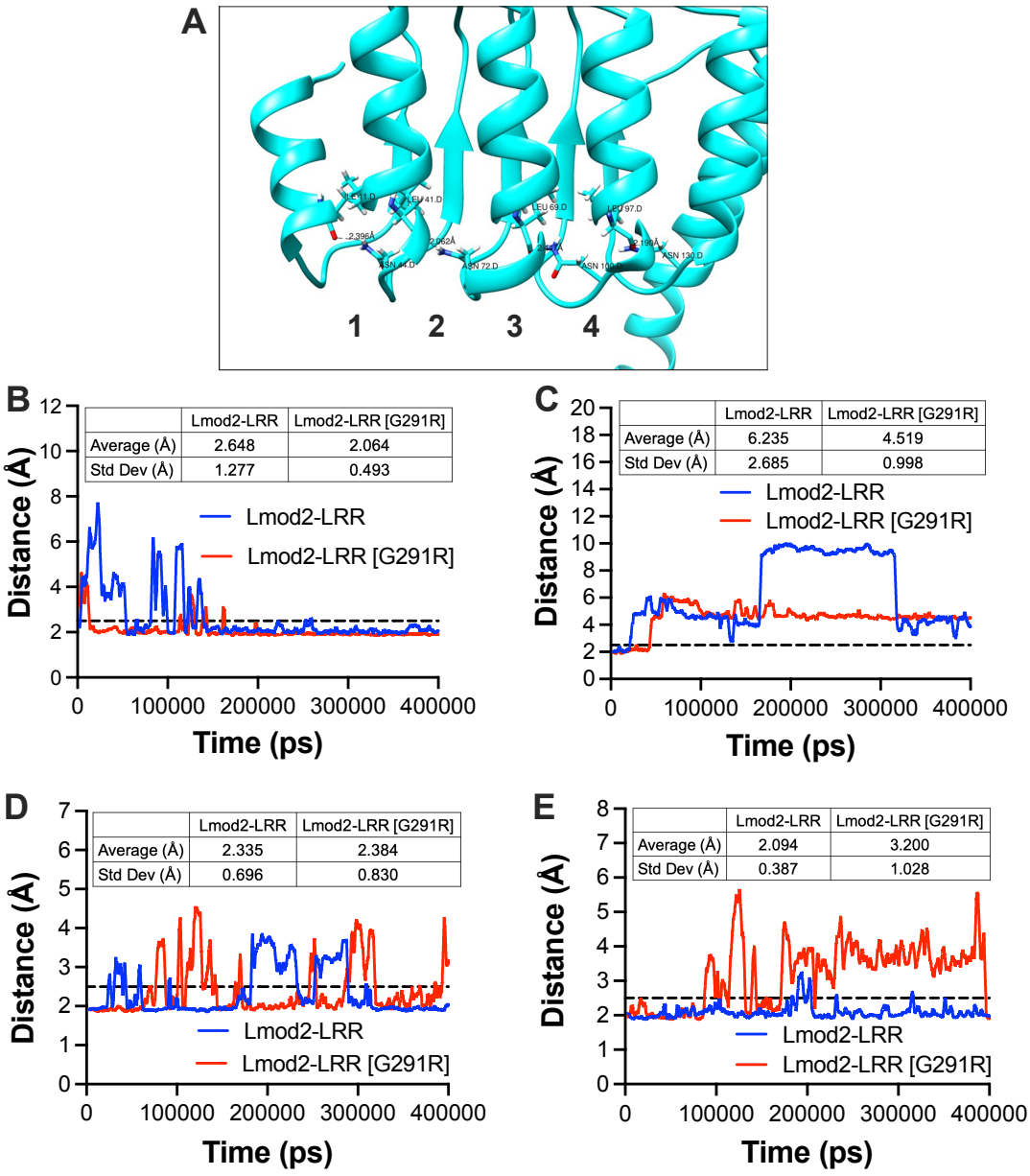

Figure S3: The G-to-R mutation destabilizes nearly all asparagine ladder hydrogen bonds within the Lmod2 LRR domain. (A) Lmod2-LRR asparagine ladder hydrogen bonds in their crystal structures (PDB ID codes: 5WFN). The amino acid residues contributing hydrogen bond donors/acceptors and the distances between these atoms are labeled. Hydrogen bonds (1-4) are numbered based on their appearance in the sequence from the N-terminus. (B-E) Lmod2-LRR and Lmod2-LRR [G291R] asparagine ladder hydrogen bonding atom 2.5 nanoseconds moving average distance. (B) Hydrogen bond 1, (C) Hydrogen bond 2, (D) Hydrogen bond 3, (E) Hydrogen bond 4. Å: angstroms, Std Dev: standard deviation, ps: picoseconds, **- - - -** 2.5 Å H bond cutoff.

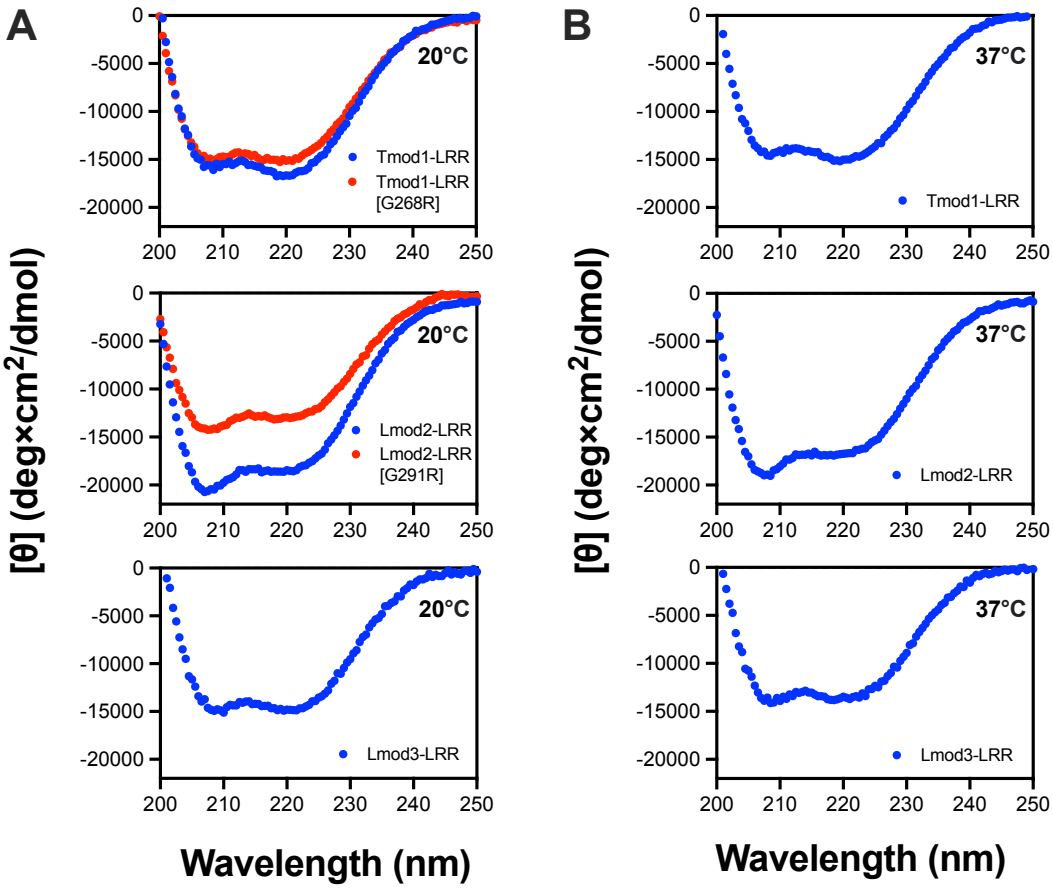

Figure S4: The G-to-R mutation disrupts the structures of Tmod and Lmod LRR domains. Circular dichroism (CD) spectra of the Tmod and Lmod WT and G-to-R mutant LRR domains were measured from 250 to 200 nm in 10 mM sodium phosphate, pH 7.6 at (A) 20°C or at (B) 37°C. Blue indicates WT LRR domains, red indicates G-to-R mutant LRR domains. Note, due to visible aggregation CD spectra for G-to-R mutants cannot be measured at 37°C for Tmod1 and Lmod2 and both at 20°C and 37°C for Lmod3.

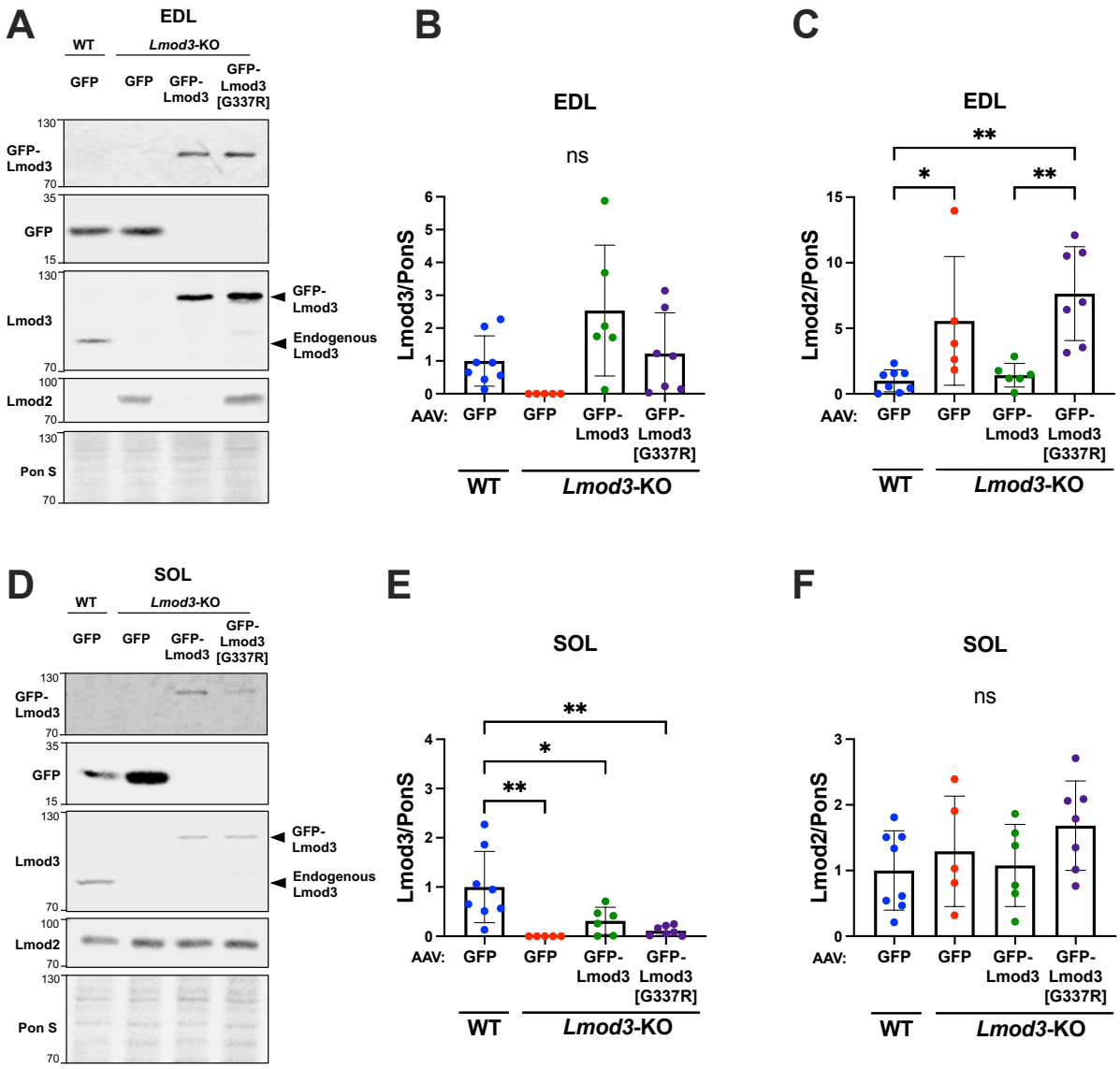

Figure S5. Lmod2 expression is upregulated in the EDL of *Lmod3*-KO mice expressing GFP-AAV control and GFP-Lmod3 [G337R]-AAV. Immunoblot analysis of Lmod3 and Lmod2 protein levels in the extensor digitorum longus (EDL) and soleus (SOL) muscles of WT and *Lmod3*-KO mice. Mice were injected with adeno-associated virus expressing either GFP, GFP-Lmod3, or GFP-Lmod3 [G337R]. (A) Representative blots of (A) EDL and (D) SOL muscle tissue lysate from a single animal per each group probed with anti-Lmod3, anti-GFP, or anti-Lmod2 antibodies. Mean relative protein expression of (B, E) Lmod3 and (C, F) Lmod2 ± SD; All analyses are of PD20-22 mice. n=5–8 mice per group, *p<0.05, **p<0.01, ns: not significant, one-way ANOVA.

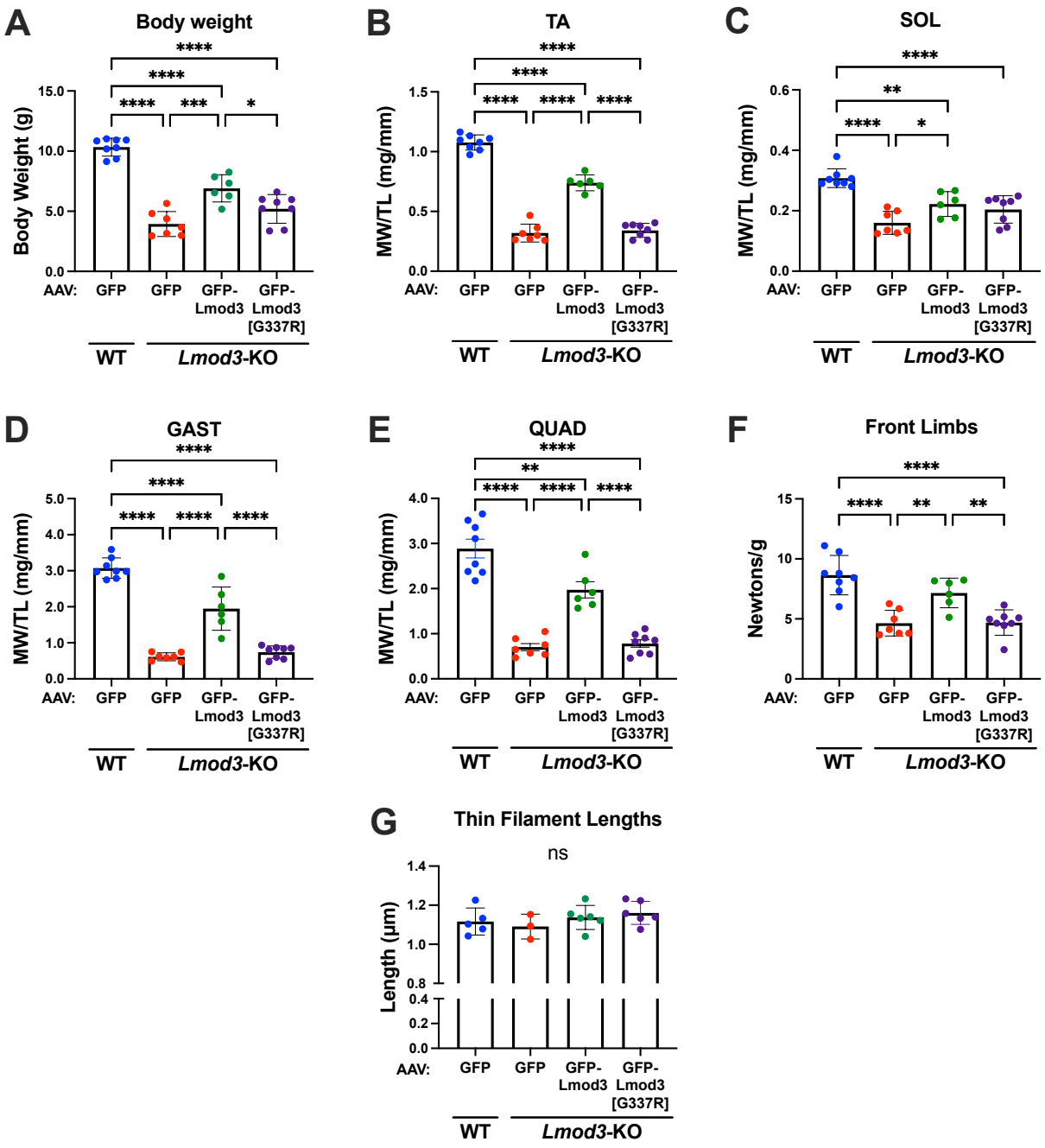

Figure S6. Expression of GFP-Lmod3, but not GFP-Lmod3 [G337R], improves body and muscle weights, grip strength, and motor coordination of *Lmod3*-KO mice. (A) Raw body weight in grams (g), (B) tibialis anterior (TA), (C) soleus (SOL), (D) gastrocnemius (GAST), (E) quadriceps (QUAD) muscle weight (MW) normalized to tibia length (TL) in mg/mm, (F) grip strength from the front limbs, (G) thin filament lengths taken from soleus muscle tissue. All measurements were analyzed from PD21 mice. (A-F) n=6-8 mice per group, (G) n=3-6 mice per group, Mean ± SD, *p<0.05, **p<0.01, ***p<0.001, ****p<0.0001, one-way ANOVA.

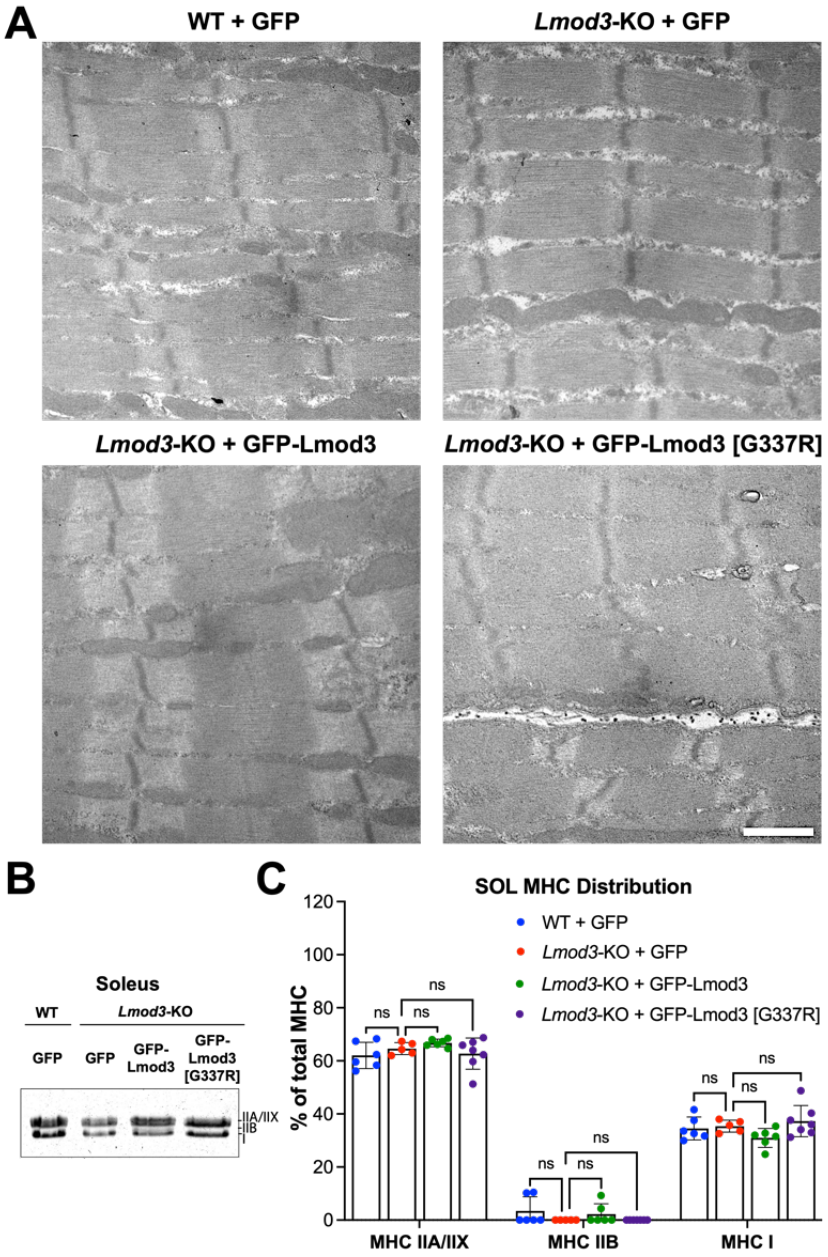

Figure S7. Sarcomeric organization and myosin heavy chain (MHC) isoform expression are unaltered in the SOL muscle of the *Lmod3*-KO mice. A) Representative images of fixed SOL muscle sections taken by transmission electron microscopy (scale bar = 1 μm). (B) 8% Poly-acrylamide SDS-gel showing myosin heavy chain (MHC) distribution (top: type IIA/IIX, middle: type IIB, bottom: type I) after separation by electrophoresis in the SOL muscle from WT or *Lmod3*-KO mice expressing either GFP, GFP-Lmod3, or GFP-Lmod3 [G337R]. (C) Quantification of MHC distribution in the SOL muscle is shown as a percent of total myosin. Mean ± SD, n=5-7 mice per group, two-way ANOVA, ns: not significant.

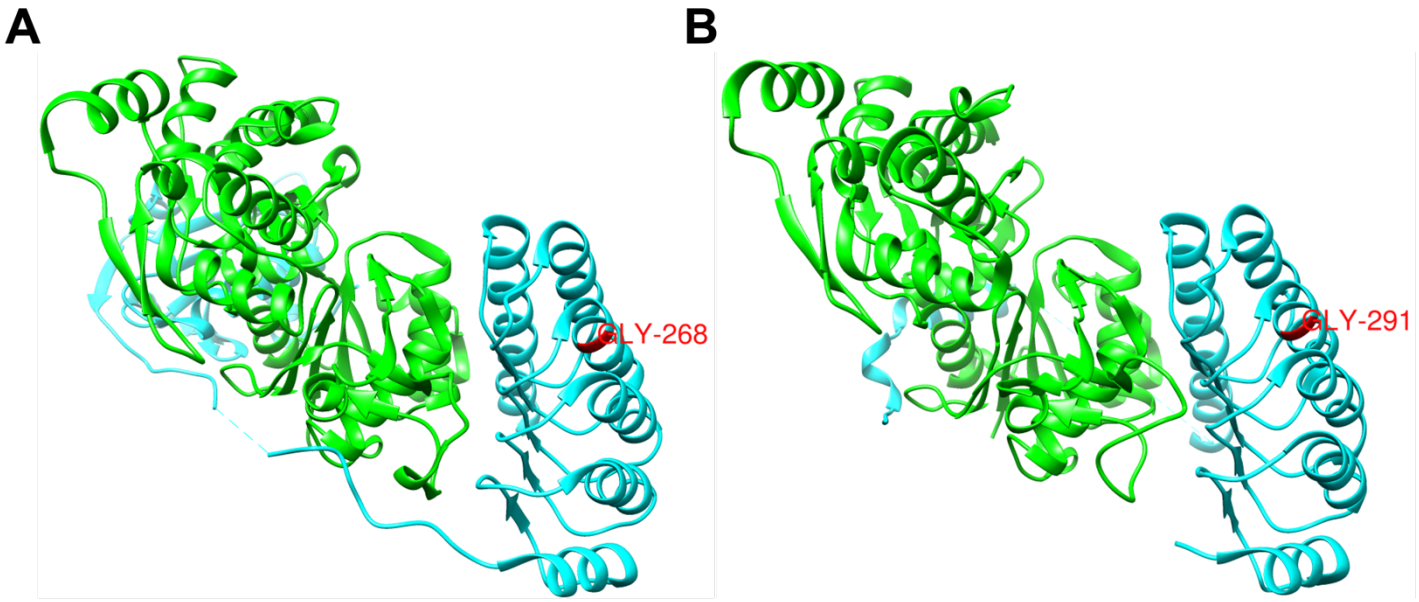

Figure S8. The glycine residue affected by the G-to-R mutation is positioned away from the actin/Tmod1 or actin/Lmod2 binding interface. The crystal structures of (A) Tmod1-LRR and actin complex (PDB 4PKI) and (B) Lmod2-LRR and actin complex (PDB 5WFN). The glycine (Gly) residue affected by the G-to-R mutation in either molecule is highlighted and labeled in red. The LRR ribbons are in cyan, and the actin ribbons are in green.

SI REFERENCES

1. Tsukada T, et al. (2011) Identification of residues within tropomodulin-1 responsible for its localization at the pointed ends of the actin filaments in cardiac myocytes. *J Biol Chem* 286(3):2194–204.
2. Liu H, Naismith JH (2008) An efficient one-step site-directed deletion, insertion, single and multiple-site plasmid mutagenesis protocol. *BMC Biotechnol* 8:91.
3. Sun Y, et al. (2015) A Human Platelet Receptor Protein Microarray Identifies the High Affinity Immunoglobulin E Receptor Subunit α (FcεR1α) as an Activating Platelet Endothelium Aggregation Receptor 1 (PEAR1) Ligand. *Mol Cell Proteomics* 14(5):1265–74.
4. Pardee JD, Aspudich J (1982) Purification of Muscle Actin. *Methods Enzymol*. doi:10.1016/0076-6879(82)85020-9.
5. Kostyukova AS, Hitchcock-DeGregori SE (2004) Effect of the structure of the N terminus of tropomyosin on tropomodulin function. *J Biol Chem* 279(7):5066–71.
6. Colpan M, et al. (2016) Tropomyosin-binding properties modulate competition between tropomodulin isoforms. *Arch Biochem Biophys* 600:23–32.
7. Colpan M, Iwanski J, Gregorio CC (2021) CAP2 is a regulator of actin pointed end dynamics and myofibrillogenesis in cardiac muscle. *Commun Biol* 4(1):365.
8. Chereau D, et al. (2008) Leiomodin is an actin filament nucleator in muscle cells. *Science* 320(5873):239–43.
9. Ramos JN, et al. (2019) Development of Novel Micro-dystrophins with Enhanced Functionality. *Mol Ther*. doi:10.1016/j.ymthe.2019.01.002.
10. Pappas CT, et al. (2015) Knockout of Lmod2 results in shorter thin filaments followed by dilated cardiomyopathy and juvenile lethality. *Proc Natl Acad Sci*. doi:10.1073/pnas.1508273112.
11. Cenik BK, et al. (2015) Severe myopathy in mice lacking the MEF2/SRF-dependent gene leiomodin-3. *J Clin Invest* 125(4):1569–78.
12. Washabaugh CH, Ontell MP, Kant JA, Ontell M (1999) Creatine kinase transcript accumulation: effect of nerve during muscle development. *Dev Dyn* 215(4):285–96.
13. Pappas CT, Bhattacharya N, Cooper JA, Gregorio CC (2008) Nebulin interacts with CapZ and regulates thin filament architecture within the Z-disc. *Mol Biol Cell*. doi:10.1091/mbc.E07-07-0690.

1. Tsukada T, et al. (2011) Identification of residues within tropomodulin-1 responsible for its localization at the pointed ends of the actin filaments in cardiac myocytes. *J Biol Chem* 286(3):2194–204.
2. Liu H, Naismith JH (2008) An efficient one-step site-directed deletion, insertion, single and multiple-site plasmid mutagenesis protocol. *BMC Biotechnol* 8:91.
3. Sun Y, et al. (2015) A Human Platelet Receptor Protein Microarray Identifies the High Affinity Immunoglobulin E Receptor Subunit α (FcεR1α) as an Activating Platelet Endothelium Aggregation Receptor 1 (PEAR1) Ligand. *Mol Cell Proteomics* 14(5):1265–74.
4. Pardee JD, Aspudich J (1982) Purification of Muscle Actin. *Methods Enzymol*. doi:10.1016/0076-6879(82)85020-9.
5. Kostyukova AS, Hitchcock-DeGregori SE (2004) Effect of the structure of the N terminus of tropomyosin on tropomodulin function. *J Biol Chem* 279(7):5066–71.
6. Colpan M, et al. (2016) Tropomyosin-binding properties modulate competition between tropomodulin isoforms. *Arch Biochem Biophys* 600:23–32.
7. Colpan M, Iwanski J, Gregorio CC (2021) CAP2 is a regulator of actin pointed end dynamics and myofibrillogenesis in cardiac muscle. *Commun Biol* 4(1):365.
8. Chereau D, et al. (2008) Leiomodin is an actin filament nucleator in muscle cells. *Science* 320(5873):239–43.
9. Ramos JN, et al. (2019) Development of Novel Micro-dystrophins with Enhanced Functionality.

Mol Ther. doi:10.1016/j.ymthe.2019.01.002.
10. Pappas CT, et al. (2015) Knockout of Lmod2 results in shorter thin filaments followed by dilated cardiomyopathy and juvenile lethality. *Proc Natl Acad Sci*. doi:10.1073/pnas.1508273112.
11. Cenik BK, et al. (2015) Severe myopathy in mice lacking the MEF2/SRF-dependent gene leiomodin-3. *J Clin Invest* 125(4):1569–78.
12. Washabaugh CH, Ontell MP, Kant JA, Ontell M (1999) Creatine kinase transcript accumulation: effect of nerve during muscle development. *Dev Dyn* 215(4):285–96.
13. Pappas CT, Bhattacharya N, Cooper JA, Gregorio CC (2008) Nebulin interacts with CapZ and regulates thin filament architecture within the Z-disc. *Mol Biol Cell*. doi:10.1091/mbc.E07-07-0690.